Structures 63 (2024) 106476

Contents lists available at ScienceDirect

Structures

journal homepage: www.elsevier.com/locate/structures

Modelling of flexural fatigue behaviours of hybrid engineered cementitious composite link slabs using cycle-driven analysis

Shiyao Zhu [a], Y.X. Zhang [b], C.K. Lee [a,*]

[a] School of Engineering and Technology, University of New South Wales, Canberra, ACT 2600, Australia
[b] School of Engineering, Design and Built Environment, Western Sydney University, Kingswood, NSW 2751, Australia

ARTICLE INFO

Keywords:
Cycle-driven analysis
Engineered cementitious composite (ECC)
Link slabs
Finite element modelling
High-cycle fatigue failure
Residual strength

ABSTRACT

Link slabs are designed and expected to be serviced under high-cycle traffic loadings. Although their high-cycle fatigue performance is critical in their practical applications, very few experimental and numerical studies have been conducted to study high-cycle fatigue failure of link slabs due to the huge amount of time and resources needed for fatigue tests and the lack of efficient modelling method for high-cycle fatigue failure. Recently, as a newly developed material with superior mechanical properties, the hybrid fibre reinforced engineered cementitious composite (hybrid ECC) has been recommended for link slab application. In this study, a novel and efficient cycle-driven analysis (CDA) procedure was developed to model the structural behaviour of ECC link slabs made of the hybrid ECC under high-cycle fatigue loadings, which is the first attempt for CDA to be applied in high-cycle fatigue structural modelling of a hybrid ECC link slab with reinforcement bars. In the proposed CDA, fatigue damages of both hybrid ECC and reinforcement bars were taken into account. The accuracy and reliability of the new CDA procedure were validated by comparing the modelling predictions with the experimental results on two quarter-scaled hybrid ECC link slabs. It was found that the proposed CDA procedure could predict the overall fatigue behaviours including the deflection histories, crack patterns, fatigue life, fatigue failure mode and the residual static strength of the hybrid ECC link slabs after fatigue damage with good accuracy.

1. Introduction

Engineered cementitious composites (ECCs) have been attracting growing interest in structural beam and slab applications due to their superior mechanical properties [1–3]. For link slab applications, as the slabs are supposed to withstand repeated traffic loadings, high-cycle fatigue performance is one of the most critical factors affecting the service life of the slabs. Recently, a hybrid fibre reinforced ECC (hybrid ECC) with polyethylene and steel fibres has been developed to meet the high-cycle fatigue demand of such applications [4]. The hybrid ECC achieved a balanced performance of strength and ductility among mono fibre ECCs [4,5]. In addition, a series of four-point bending tests showed that the hybrid ECC had excellent crack width control ability under static and fatigue flexural loadings [5].

In order to assess the structural performance of ECC link slabs under fatigue loading, high-cycle fatigue tests are usually conducted [2,3,6]. However, such tests are very costly, time consuming and are only able to investigate the fatigue behaviours of a given design under one specific loading condition. Worst still, while most studies usually tested up to two million cycles due to time limits [2,3], in practice, millions of loading cycles are required to assess the performance of the slab under service loading. According to an equivalent single axle load (ESAL) calculation with a service life of 20 years [6,7], it is estimated that for a laboratory test with a typical 4 Hz loading frequency setup, at least 76 days of continuous testing is required to complete a single fatigue test on a link slab.

Numerical modelling methods such as the finite element (FE) method have been demonstrated to be an effective approach for structural analysis, and it has been employed to complement the costly experimental studies for investigating the structural performance of beams and slabs under static loading [8–13]. However, due to the lack of suitable material damage model for high-cycle fatigue loading, even for reinforced concrete structures which have been used in structural applications for many decades, relatively few numerical studies have been carried out to predict their structural responses under high-cycle fatigue loading [14,15]. Towards this end, even fewer numerical studies have

* Corresponding author.
E-mail address: chi.k.lee@unsw.edu.au (C.K. Lee).

https://doi.org/10.1016/j.istruc.2024.106476
Received 3 December 2023; Received in revised form 6 April 2024; Accepted 22 April 2024
Available online 27 April 2024

been devoted to model the fatigue behaviour of beams and slabs constructed using ECC, which is a relatively new but very promising construction material for enhanced structural performance under fatigue loading. One of the main reasons is that a comprehensive fatigue damage model of ECC is largely unavailable. In addition, the effect of analysis cycles on the modelling accuracy is still unclear. Some preliminary studies have been attempted to consider fatigue damage of fibre reinforced concrete when simulating of flexural fatigue properties at material level [16,17]. Cachim [16] introduced cycle-dependent plastic strain to model the fatigue damage of steel fibre reinforced concrete based on the viscoplasticity theory. Banjara and Ramanjaneyulu [17] modelled the damage of fibre reinforced concrete using a fictitious model with fracturing strains introduced. In these models, some analytical parameters are required to be determined by trial and error for fitting the experimental data, which may not be practical for fatigue analysis. In addition, although the fatigue simulations were running with increments of a number of cycles, the effect of applied increments on the accuracy of the analysis was still unclear [16,17].

Recently, a cycle-driven analysis (CDA) procedure was proposed by Zhu et al. [18] for modelling the flexural fatigue performance of hybrid ECC materials under four-point fatigue bending loading and its accuracy was validated with fatigue tests. This proposed CDA procedure simplified the fatigue analysis and greatly reduced the computational resource needed for fatigue modelling of hybrid ECCs materials by replacing cycle-by-cycle analysis with a small number of equivalent static FE analyses. Based on the three-stage damage law [19] which stated that the damage of ECC material was developed linearly at the major second fatigue stage which contributed to most of the fatigue life of the modelling material, the CDA skipped most fatigue loading cycles during the analysis. It was found that less than fifty equivalent static analyses were adequate to capture the flexural fatigue behaviours of hybrid ECC small beams subjected to two million fatigue loading cycles [18].

In this study, in order to predict the structural performance and behaviours of a hybrid ECC link slabs with steel reinforcement bars subject to high-cycle fatigue loading, a new damage model and a new failure criterion for reinforcement bars were introduced to the original CDA procedure [18]. Fatigue damages of both hybrid ECC and steel reinforcement bars were considered in the new CDA models developed in this paper. This new CDA procedure is the first attempt to provide an efficient and numerical modelling for predicting the detailed structural responses of a hybrid ECC link slab under high-cycle fatigue loadings. In order to present this new CDA procedure, the general concept of CDA was first summarized and the termination/failure criteria for link slabs applications were then defined. After these, the material damage models of hybrid ECC and the steel reinforcement bar adopted in the new CDA were described. The proposed new CDA procedure was then employed to predict the fatigue behaviours of two quarter-scaled hybrid ECC link slabs subjected to different fatigue loading scenarios [6]. The accuracy and reliability of the new CDA procedure were validated by comparing the predicted fatigue behaviours of the modelled slabs with the corresponding test results reported in [6]. The detailed structural behaviours were simulated, including deflection history, crack pattern, fatigue life, failure mode and the residual static strength of the hybrid ECC link slabs after fatigue damage, which showed the practicability of the extended CDA procedure for engineering structural analysis.

2. General concept of cycle-driven analysis (CDA)

The original cycle-driven analysis (CDA) was proposed for the analysis of flexural fatigue properties of the hybrid ECC materials developed by Zhu et al. [18]. It is implemented by using the FE analysis (FEA) software platform ABAQUS [20]. As shown in the right-hand side of Fig. 1, the proposed CDA procedure is composed of five main steps, namely (i) input of analysis parameters, (ii) creation of the baseline FE model, (iii) FE analysis and damage update, (iv) checking of termination criteria, and (v) output of analysis results [18]. Among these steps, steps

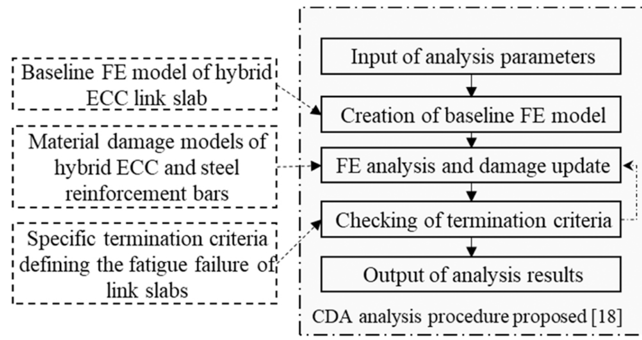

Fig. 1. Adapted CDA procedure for structural analysis on link slabs.

(iii) and (iv) will be repeated until the termination criteria are met in step (v). As a result, by accounting for the fatigue damages with increasing cycles, the fatigue behaviour could be simulated by a series of static FE analyses.

In order to extend the original CDA procedure for structural analysis of link slabs under fatigue loading, in addition to the damage model of ECC which had been described in [18], the material damage model of steel reinforcement bars and a new set of termination criteria defining fatigue failure of link slab are required (left-hand side of Fig. 1). The baseline FE model of link slabs used in this study included the reinforcement bars details and support conditions. The accuracy of the baseline FE model used is first validated against the experimental results obtained from a static test. The detailed theoretical background, analysis steps and damage update approach used in the CDA procedure are given in [18]. Therefore, a detailed description of the CDA will not be repeated here and only a summary will be given in Sections 2.1 and 2.2 with highlights on those additional features used in link slab analysis.

2.1. CDA for link slab analysis

Fig. 2 shows the overview of the extended CDA procedure for predicting the structural behaviour (e.g., the displacement-cycle curve shown in Fig. 2c) of hybrid ECC link slabs under fatigue loading. As shown in Fig. 2a, a series of FE models $\boldsymbol{M} = [M_1, M_2, M_3, \ldots, M_J]$ of the link slab are created corresponding to a number of predefined load cycles $\boldsymbol{N} = [N_1, N_2, N_3, \ldots, N_J]$. Note that for any two integers $I1$ and $I2$ such that $1 \le I1 \le J$ and $1 \le I2 \le J$, if $I2 > I1$ then $N_{I2} > N_{I1}$. These predefined analysis cycles $N = [N_1, N_2, N_3, \ldots, N_J]$ are part of the applied cycles within the fatigue life (or load cycle applied to the actual structure in a fatigue test) of the link slab distributed at certain intervals. As shown in Fig. 2b, N_1, N_K, and N_J correspond to the first cycle, a typical load cycle within the fatigue life and the last cycle of analysis, respectively. To initiate the CDA, at $j = 1$, an undamaged FE model M_1 (the red model in Fig. 2a) is created for the first load cycle $N_1 = 1$. FE analysis is then conducted using the first model M_1. The load-deformation relation (red line in Fig. 2b) and damages of ECC materials and steel reinforcement bars will then be retrieved from the FE analysis results. It should be noted that based on the hybrid ECC and steel reinforcement bar damage models (described in Section 3), the damage distribution of the link slab will be defined and retrieved from the modelling result of M_1. This damage distribution will then be employed in the next FE model (M_2) at the next analysis step $j = 2$ corresponding to the cycle N_2. Similarly, as j increases, the damage distribution defined and retrieved from the previous FE analysis (M_2) is employed in the next FE model (M_3) for $j = 3$ and cycle N_3 and so on. As the CDA procedure is continued, more damage will be induced to the FE models. For example, the model M_K (blue model in Fig. 2a) at cycle N_K (blue line in Fig. 2b) will have a higher deflection than M_1 while the last model M_J created during the CDA (green model in Fig. 2a) corresponding to the last analysis cycle N_J (green line in Fig. 2b) will result in a higher deflection than M_K. Since the damages are considered in each model as the applied cycle increases, the

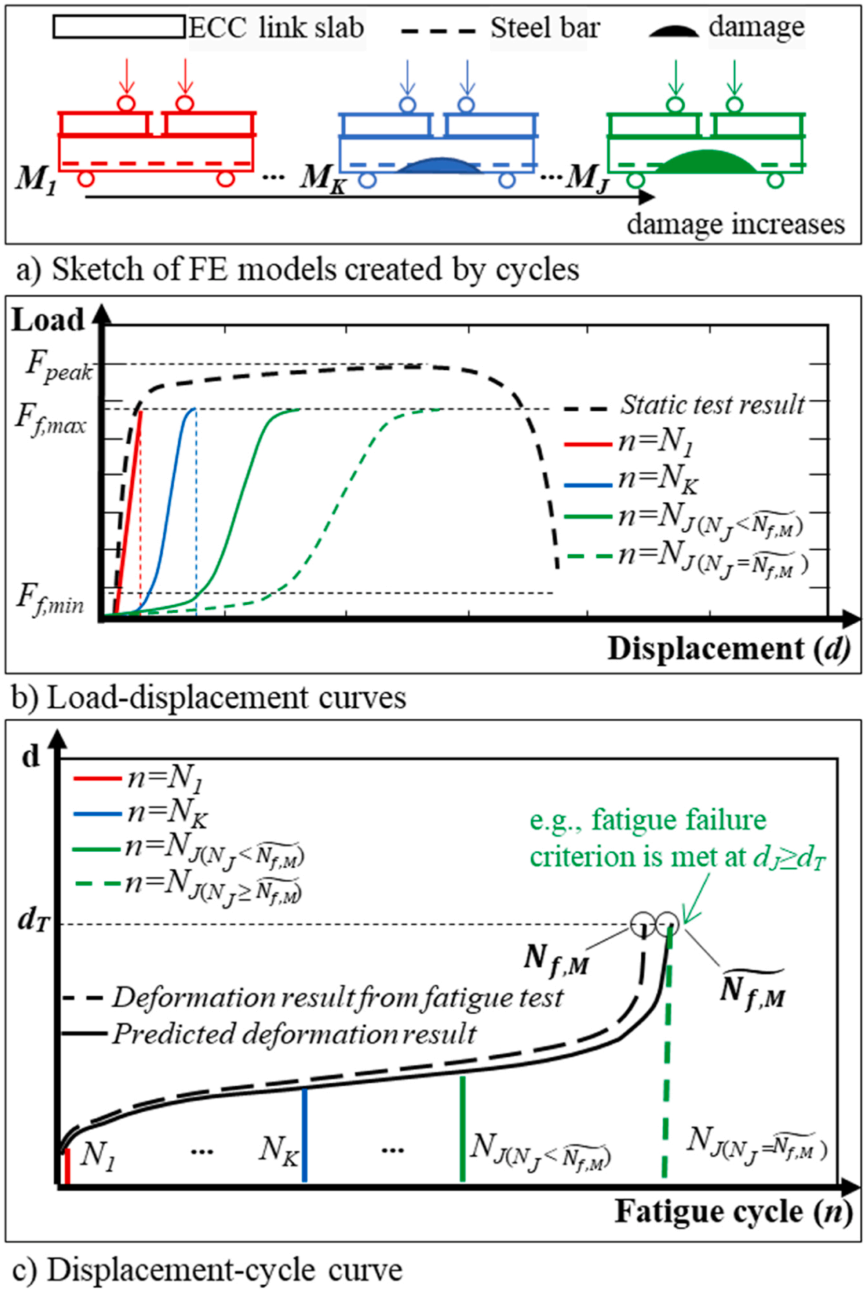

Fig. 2. Schematic diagram of CDA.

damage accumulation process is simulated and thus the fatigue behaviour of the link slab can be predicted. For each static analysis, loading is applied from zero to the maximum applied fatigue load $F_{f,max}$. By conducting a series of static FE analyses, the corresponding load-displacement curves are obtained as illustrated in Fig. 2b. Furthermore, as shown in Fig. 2c, by connecting the deformations at $F_{f,max}$ from these static analyses, the displacement-cycle curve is obtained.

Due to the design of the CDA, the number of FE models required for fatigue analysis is significantly reduced from N_J (the number of fatigue cycles applied in the tests which could be equal to millions for a link slab under service loading) to J (the number of equivalent static analyses conducted which is normally less that one hundred). In addition, the accuracy of the CDA is related to the analysis cycle intervals selected i.e. $\boldsymbol{N} = [N_1, N_2, N_3, \ldots, N_J]$. In the design of CDA [18], the analysis sequence $\boldsymbol{N}$ is controlled by two parameters ΔN_{min} and ΔN_{maj} corresponding to the initial/final failure stage and the linear fatigue stage of the structure, respectively. Values of ΔN_{min} and ΔN_{maj} can be controlled by a user defined density factor k. In [18], it is found that a value of $k = 10$ or 15 could usually lead to good modelling accuracy even for high-cycle fatigue failure tests that involve millions of load cycles. By using suitable cycle intervals (i.e., an appropriate density factor k), as shown in Fig. 2c, CDA can predict the estimated fatigue life ($\widetilde{N_{f,M}}$) of the link slab so that $N_J=\widetilde{N_{f,M}}$. That is, the CDA is stopped when fatigue failure has been detected so that the user defined failure/termination criteria are reached (the green dashed line Fig. 2c). It should be noted that as the modelling prediction is not perfect, the actual fatigue life $N_{f,M}$ may be less or greater than the predicted fatigue life $\widetilde{N_{f,M}}$. Fig. 2c actually shows the case that $\widetilde{N_{f,M}} > N_{f,M}$. Furthermore, one of the advantages of the CDA is that it also allows users to simulate the fatigue behaviour up to any interested cycles before fatigue failure has occurred (i.e., before the user defined failure/termination criteria are reached, green solid line

Fig. 2c). In this case, the final analysis model M_J will contain the latest damaged information of the link slab so that a static FE analysis of M_J should allow the user to evaluate the static residual strength of the link slab after certain fatigue cycles are sustained.

2.2. Analysis termination criteria

In Zhu et al.'s work [18], when applying CDA for flexural fatigue analysis on small hybrid ECC beams under four-point bending, an analysis termination criterion of $d_J \geq d_T$ was used, where d_J is the midspan deflection of the beam at cycle N_J and d_T is the midspan deflection limit. In this study, the original CDA is extended to conduct structural fatigue analysis of an ECC link slab with steel reinforcement bars. Since for an ECC link slab, fatigue failure could be caused by either (i) the fatigue failure of the ECC matrix or (ii) the fatigue failure of the steel reinforcement bars, two termination criteria are proposed in this study. The first termination criterion is the deformation limit of the link slab so that the slab is considered failed whenever $d_J \geq d_T$. This criterion is employed to identify the failure of the hybrid ECC matrix as the midspan deflection of the link slab is highly dependent on the fatigue damage of the ECC matrix. For the fatigue failure of reinforcement bars, the termination criterion of $D_{bar,J} \geq 1.0$, where $D_{bar,J}$ is the normalised damage index D_{bar} at cycle N_J, is used. A detailed definition of D_{bar} will be given in Section 3.2. CDA will be stopped whenever any of these two criteria is first met. Furthermore, by noticing which criterion is first met, the failure mode of the link slab can also be identified.

3. Material and damage models

Material and damage models of the hybrid ECC and the steel reinforcement bars used in the CDA of ECC link slab are described in this section. It should be noted that the material models under static loading will be employed in the baseline FE models (i.e., M_1) before any fatigue damage is developed. While the material damage models will be employed to describe the stress-strain behaviour of the materials after fatigue damage occurred (i.e., for models M_2 to M_J).

3.1. Material and damage models of hybrid ECC

As shown in Fig. 3, a multilinear curve is employed to define the compressive stress-strain relationship of hybrid ECC under static loading [21]. The model used is expressed as

$$\sigma = \begin{cases} E\varepsilon & 0 \leq \varepsilon < \varepsilon_{0.4} \\ E\varepsilon(1-\alpha_0) & \varepsilon_{0.4} \leq \varepsilon < \varepsilon_{c0} \\ \alpha_1(\varepsilon - \varepsilon_{c0}) + \sigma_{c0} & \varepsilon_{c0} \leq \varepsilon < \varepsilon_{cl} \\ \alpha_2(\varepsilon - \varepsilon_{cl}) + \sigma_{cl} & \varepsilon_{cl} \leq \varepsilon < \varepsilon_{cm} \end{cases} \tag{1}$$

In Eq. 1, E is the Young's modulus of the hybrid ECC. $\varepsilon_{0.4}$, ε_{c0}, ε_{cl}, and ε_{cm} are the compressive strain at the end of the elastic stage (point A), the ultimate strength (point B), the inflection point at the softening stage (point C), and the end of softening stage (point D). σ_{c0} and σ_{cl} are the stress corresponding to the strain ε_{c0} and ε_{cl}, respectively. α_0, α_1, and α_2 are material parameters determined by linear regression analysis from standard compression tests [22].

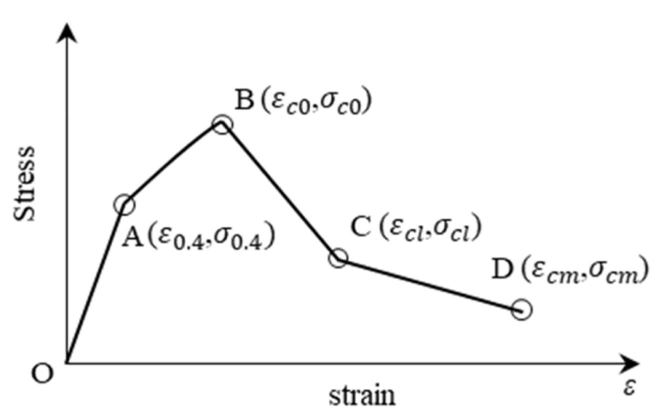

Fig. 3. Stress-strain relationship of hybrid ECCs under compression.

As shown in the black solid line of Fig. 4, the multilinear model defines the tensile stress-strain relationship of the hybrid ECC under static loading [21], which is expressed as

$$\sigma_t = \begin{cases} E\varepsilon & 0 \leq \varepsilon < \varepsilon_{t0} \\ \sigma_{t0} + (\sigma_{t1} - \sigma_{t0})\left(\dfrac{\varepsilon - \varepsilon_{t0}}{\varepsilon_{t1} - \varepsilon_{t}}\right) & \varepsilon_{t0} \leq \varepsilon < \varepsilon_{t1} \\ \sigma_{t1} + (\sigma_{tp} - \sigma_{t1})\left(\dfrac{\varepsilon - \varepsilon_{t1}}{\varepsilon_{t1} - \varepsilon_{t1}}\right) & \varepsilon_{t1} \leq \varepsilon < \varepsilon_{tp} \\ \sigma_{tp}\left(1 - \dfrac{\varepsilon - \varepsilon_{tp}}{\varepsilon_{tu} - \varepsilon_{tp}}\right) & \varepsilon_{tp} \leq \varepsilon < \varepsilon_{tu} \end{cases} \tag{2}$$

In Eq. 2, ε_{t0}, ε_{t1}, ε_{tp}, and ε_{tu} are the tensile strains at the elastic limit (point A), the inflection point at the hardening stage (point B), the peak stress (point C), and the end of softening stage (point D). σ_{t0}, σ_{t1}, σ_{tp} and σ_{tu} are correspondingly the stress at the strains ε_{t0}, ε_{t1}, ε_{tp}, and ε_{tu}, respectively. These material parameters are obtained by direct tensile tests using dog bone specimens [4,23].

The material damage model developed by Zhu et al. [18] is employed to describe the stress-strain behaviour of hybrid ECC after fatigue damage occurred. The fatigue damage model is determined by the degraded stiffness E_n and the accumulated plastic strain $\varepsilon_{Apl,n}$. The stress-strain curve (Fig. 4) under static loading is employed as the backbone strength envelope. It is assumed after n cycles of fatigue loading, that the damage is induced and therefore the material stiffness will be reduced to E_n and some plastic strain $\varepsilon_{Apl,n}$ will be accumulated. Therefore, as more plastic strain $\varepsilon_{Apl,n}$ develops with the increase of damage, the corresponding stress-strain curve will be defined by a different set of equations given in Eqs. 3 to 5.

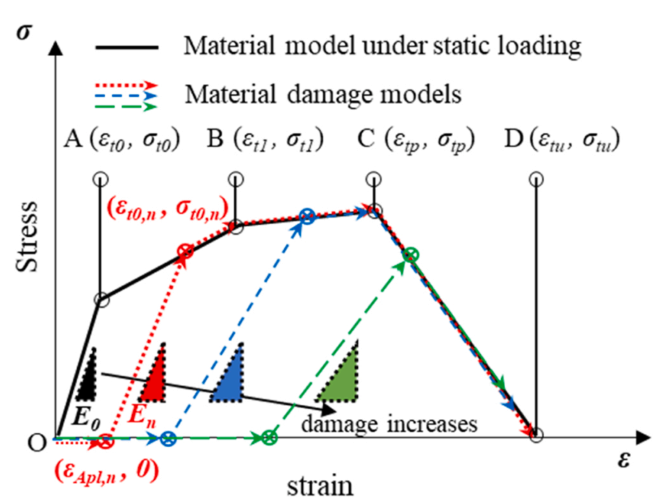

Fig. 4. Stress-strain relationship of hybrid ECCs under tension.

$$\sigma_t = \begin{cases} 0 & 0 \le \varepsilon < \varepsilon_{Apl,n} \\ E_n \varepsilon & \varepsilon_{Apl,n} \le \varepsilon < \varepsilon_{t0,n} \\ \sigma_{t0,n} + (\sigma_{t1} - \sigma_{t0,n})\left(\dfrac{\varepsilon - \varepsilon_{t0,n}}{\varepsilon_{t1} - \varepsilon_{t0,n}}\right) & \varepsilon_{t0,n} \le \varepsilon < \varepsilon_{t1} \\ \sigma_{t1} + (\sigma_{tp} - \sigma_{t1})\left(\dfrac{\varepsilon - \varepsilon_{t1}}{\varepsilon_{t1} - \varepsilon_{t1}}\right) & \varepsilon_{t1} \le \varepsilon < \varepsilon_{tp} \\ \sigma_{tp}\left(1 - \dfrac{\varepsilon - \varepsilon_{tp}}{\varepsilon_{tu} - \varepsilon_{tp}}\right) & \varepsilon_{tp} \le \varepsilon < \varepsilon_{tu} \end{cases} \tag{3}$$

$$\sigma_t = \begin{cases} 0 & 0 \le \varepsilon < \varepsilon_{Apl,n} \\ E_n \varepsilon & \varepsilon_{Apl,n} \le \varepsilon < \varepsilon_{t0,n} \\ \sigma_{t0,n} + (\sigma_{tp} - \sigma_{t0,n})\left(\dfrac{\varepsilon - \varepsilon_{t0,n}}{\varepsilon_{tp} - \varepsilon_{t0,n}}\right) & \varepsilon_{t0,n} \le \varepsilon < \varepsilon_{tp} \\ \sigma_{tp}\left(1 - \dfrac{\varepsilon - \varepsilon_{tp}}{\varepsilon_{tu} - \varepsilon_{tp}}\right) & \varepsilon_{tp} \le \varepsilon < \varepsilon_{tu} \end{cases} \tag{4}$$

$$\sigma_t = \begin{cases} 0 & 0 \le \varepsilon < \varepsilon_{Apl,n} \\ E_n \varepsilon & \varepsilon_{Apl,n} \le \varepsilon < \varepsilon_{t0,n} \\ \sigma_{t0,n}\left(1 - \dfrac{\varepsilon - \varepsilon_{t0,n}}{\varepsilon_{tu} - \varepsilon_{t0,n}}\right) & \varepsilon_{t0,n} \le \varepsilon < \varepsilon_{tu} \end{cases} \tag{5}$$

In Eqs. 3 to 5, E_n and $\varepsilon_{Apl,n}$ are the reduced stiffness and accumulated plastic strain of the damaged ECC after n cycles of fatigue load. They are calculated by using damage indexes D_E and D_ε shown in Eqs. 6 and 7, respectively. Eqs. 8 and 9 are used for calculating damage indexes D_E and D_ε [18].

$$E_n = D_E \times E_0 \tag{6}$$

$$\varepsilon_{Apl,n} = D_\varepsilon \times \varepsilon_{tp} \tag{7}$$

$$D_E = \left(1 - \left(\frac{n}{N_f}\right)^{f_m}\right)^{f_n} \tag{8}$$

$$D_\varepsilon = 1 - \left(1 - \left(\frac{n}{N_f}\right)^{f_p}\right)^{f_q} \tag{9}$$

$$f_i = a_i S^{b_i} \quad (i = m, n, p, q) \tag{10}$$

$$\ln(N_f) = c \times S + g \tag{11}$$

In Eqs. 6 and 7, E_0 and ε_{tp} are the initial stiffness and ultimate strain at the peak load of the undamaged ECC, respectively. In Eqs. 8 and 9, f_i $(i = m, n, p,$ and $q)$ are shape factors and N_f is the fatigue life of the materials under bending. Both the shape factors and N_f are functions of stress ranges S as indicated in Eqs. 10 and 11. a_i, b_i $(i = m, n, p,$ and $q)$, c and g are material parameters and they can be obtained by best fitting the results obtained by four-point bending beam tests under fatigue loading [18].

3.2. Material model and fatigue damage model of steel reinforcement bars

A simple elastic-perfectly plastic model is adopted to describe the stress-strain relation of the steel reinforcement bars under static loading. This model has demonstrated good simulation results in many previous studies [13, 21, 24]. As shown in Fig. 5, this bilinear model describes the stress-strain relationship of the steel reinforcement bars under static loading. The stress develops linearly with Young's modulus E until it reaches the yield point (ε_y, f_{yield}). After that the stress keeps at f_{yield} as the strain increase.

The proposed material damage model for steel reinforcement bars

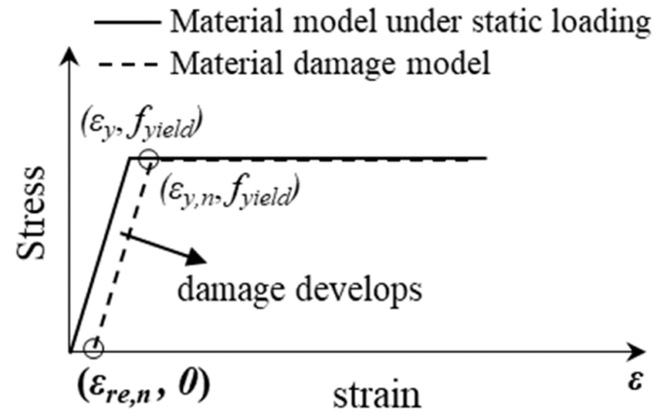

Fig. 5. Stress-strain relationship of steel reinforcement bars.

under fatigue loading (the dashed line in Fig. 5) is developed by referring to the residual plastic strains observed during actual fatigue tests [6, 25]. In this proposed damage model, degradation of stiffness is not considered as no significant reduction of stiffness of reinforcement bar was observed after damage [6]. It should be noted that after a sufficiently large number of n fatigue cycles is applied, a certain amount of residual plastic strain $\varepsilon_{re,n}$ will be developed [6,25]. As shown in Fig. 5, the dashed line describes the stress-strain relation of a steel reinforcement bar after n loading cycle and sustains a certain amount of damage. In this case, as described by Eq. 12, no stress will be developed when the strain $\varepsilon < \varepsilon_{re,n}$. After that, the stress develops linearly with Young's modulus E_s until it reaches the yield point ($\varepsilon_{y,n}$, f_{yield}) and the stress will remain constant at f_{yield} as the strain increases.

As shown in Fig. 6, the residual plastic strain is developed in a typical three-stage evolution law against the fatigue damage factor $D_{bar} = n/N_{f\text{-}bar}(S)$ [25], where n is the fatigue load cycle applied and $N_{f\text{-}bar}(S)$ is the fatigue life of the steel reinforcement bar under a given stress range S. In Stage I, the residual plastic strain fast accumulates to a small value of $\varepsilon_{re\text{-}I}$ after a small number of cycles, normally within 1 % of the fatigue life. Then it linearly increases to $\varepsilon_{re\text{-}II}$ at the end of Stage II which accounts for the most (>95 %) fatigue life. Finally, it increases to $\varepsilon_{re\text{-}III}$ suddenly in Stage III within the remaining small percentage of fatigue life. For simplification, Fig. 6 is idealized as a multilinear model as described in Eq. 13. In Eq. 13, the accumulated plastic strain $\varepsilon_{re,n}$ is developed against the damage factor D_{bar} (Eq. 14) and increased linearly in each stage. For the equation to calculate the value of $N_{f\text{-}bar}(S)$ of the typical steel reinforcement bar, it can be expressed as a function of the applied

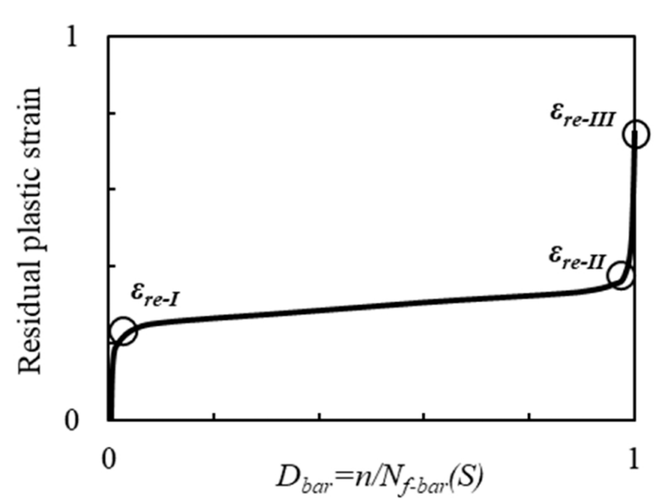

Fig. 6. Development of residual plastic strain of a typical steel reinforcement bar under a fatigue loading with stress range S.

stress range S (Eq. 15) and can be determined by using standard S-N curves given by Australian Standard [26].

$$f_t = \begin{cases} 0 & 0 \le \varepsilon < \varepsilon_{re,n} \\ E_s\varepsilon & \varepsilon_{re,n} \le \varepsilon < \varepsilon_{y,n} \\ f_{yield} & \varepsilon_{y,n} \le \varepsilon < \varepsilon_{tu} \end{cases} \tag{12}$$

$$\varepsilon_{re,n} = \begin{cases} D_{bar}/0.01 \times \varepsilon_{re-I} & D_{bar} \le 0.01 \\ \dfrac{(D_{bar}-0.01)/0.98}{(\varepsilon_{re-II}-\varepsilon_{re-I})} + \varepsilon_{re-I} & 0.01 < D_{bar} \le 0.99 \\ \dfrac{(D_{bar}-0.99)/0.01}{(\varepsilon_{re-III}-\varepsilon_{re-II})} + \varepsilon_{re-II} & 0.99 < D_{bar} \le 1 \end{cases} \tag{13}$$

$$D_{bar} = n/N_{f-bar}(S) \tag{14}$$

$$N_{f-bar}(S) = \begin{cases} (S/210)^9 \times 10^6 & S < 210MPa \\ (S/210)^5 \times 10^6 & S \ge 210MPa \end{cases} \tag{15}$$

For $\varepsilon_{re\text{-}I}$, $\varepsilon_{re\text{-}II}$, and $\varepsilon_{re\text{-}III}$ in Eq. 13 which are the residual plastic strains at the end of Stages I, II, and III, respectively (Fig. 6), their values are functions of the applied stress range S and can be determined by Eq. 16 using a linear fitting model derived from direct tensile fatigue tests [25]. In Eq. 16, u_β and v_β, $\beta = $ I, II and III are parameters to be determined from direct tensile fatigue tests.

$$\varepsilon_{re-\beta} = u_\beta S + v_\beta \quad \beta = I, II, III \tag{16}$$

4. Validation of CDA procedure for ECC link slab analysis

4.1. Tests adopted for validation of CDA

Three identical hybrid ECC link slabs [6], which were named as LS1, LS2 and LS3 respectively, were tested under both static and fatigue loadings, and the test results were used to validate the accuracy and reliability of the proposed CDA procedure. Fig. 7a shows the test setup on these three link slabs. The dimensions of the design link slab were given in Fig. 7b. For link slab LS1, it was tested under static loading (Test LS1-S in Table 1) to obtain its ultimate static strength (67.1 kN) under bending. Test results of LS1-S were used to validate the baseline FE model. Link slab LS2 was tested under two fatigue loading phases

Table 1
Summary of tests conducted by Zhu et al. [6].

Test ID	Loading program	lower load level (%)	upper load level (%)	Summary of test results
LS1-S	Static (until failure)	-		Maximum deflection of 21.1 mm observed at peak load of 67.1 kN
LS2-FI	Fatigue Phase I (ten million cycles)	1.1	11	Microcracks observed at 10,000,000th cycle with deflection of 1.49 mm.
LS2-FII	Fatigue Phase II (until failure)	7.5	75	Failure at 45,317th cycle due to fatigue failure of one of the reinforcement bars at a midspan deflection of 13.61 mm
LS3-F	Fatigue (two million cycles)	5.0	50	Microcracks observed at 2,000,000th cycle with deflection of 6.43 mm
LS3-RS	Static (until failure)	-		Maximum deflection of 16.11 mm observed at peak load of 67.7 kN

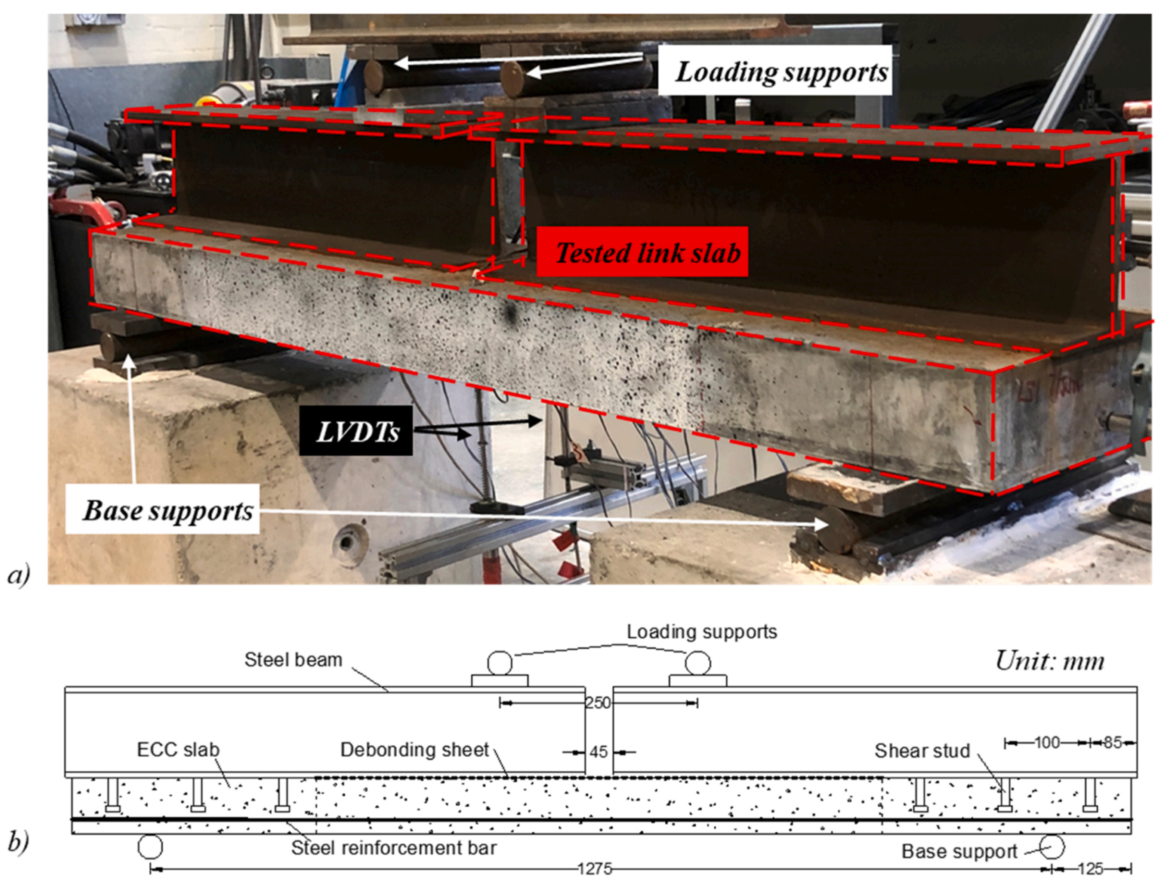

Fig. 7. a) Test setup and b) schematic diagram of link slabs LS1, LS2 and LS3.

(LS2-FI and LS2-FII in Table 1). During the fatigue tests, the midspan deflection history and fatigue failure mode were recorded. In Phase I fatigue test LS2-FI, ten million fatigue loading cycles with loading ranging from approximately 1.1 % to 11 % of the ultimate strength of link slab LS1 (0.7 kN to 7.1 kN) was applied. After the Phase I test was completed, in Phase II fatigue test LS2-FII, a higher fatigue loading ranging from approximately 7.5 % to 75 % (5.1 kN to 50.8 kN) of the ultimate static strength of link slab LS1 was applied and the test was continued until fatigue failure occurred. For link slab LS3, it was first tested with fatigue loading ranging from approximately 5 % to 50 % (3.4 kN to 33.6 kN) of the ultimate static strength of LS1 for up to two million cycles (test LS3-F in Table 1) and then followed by a static test LS3-RS to obtain the residual static strength after significant damage was induced. Table 1 summarises the program of tests and the test results. Details of the test set up and procedure can be found in [6] and they are not repeated here.

As shown in Table 2, both static FE analysis (FEA) and CDA were performed corresponding to the tests summarised in Table 1. Analysis FEA-S was conducted to validate the baseline model of the link slab by comparing the analysis results with test results from LS1-S. Three separate analyses namely CDA-11 %, CDA-50 % and CDA-75 % were performed to predict the fatigue life of the slab under the load ranges of 1.1 %− 11 %, 5 %− 50 % and 7.5 %− 75 %, respectively. In addition, an additional analysis of CDA-11 %− 1E7 was performed to investigate the development of damage and deformation of the link slab with up to ten million cycles under a fatigue load range of 1.1 %− 11 %. While CDA-50 %− 2E6 was performed to investigate the development of deformation and damage of the slab with up to two million load cycles under the fatigue load range of 5 %− 50 %. Finally, a static analysis FEA-Residual was conducted to predict the residual strength of the slab after 2 million fatigue cycles of load range of 5 %− 50 %. As shown in Table 2, the numerical analysis results were validated with corresponding test results, except for CDA-11 % and CDA-50 % where the corresponding fatigue tests for link slabs LS2 and LS3 were stopped before the slabs failed.

4.2. Validation of baseline FE model

As shown in Fig. 8, the baseline FE model was created based on the actual setup of the link slab. The FE software platform ABAQUS was employed to create the FE model. The compressive and tensile properties of the hybrid ECC adopted were given in Tables 3 and 4, respectively. The Young's modulus of steel reinforcement bars was 200 GPa and the yield strength was 500 MPa. A mesh size of 10 mm was used in the mid-section (Fig. 8) of the slab based on a mesh sensitivity study conducted in [21]. The interactions among different parts of the whole model were simulated by *Tie*, *Hard*, *Tangential*, and *Embed* models

Table 2
Summary of numerical analyses performed.

FEA/CDA ID	Analysis aim description	Validated by test
FEA-S	To verify the baseline static loading model	LS1-S
CDA-11 %	To predict the fatigue life under a load range of 1.1 % to 11 % of the ultimate strength of LS1	-
CDA-50 %	To predict the fatigue life under a load range of 5 % to 50 % of the ultimate strength of LS1	-
CDA-75 %	To predict the fatigue life under a load range of 7.5 % to 75 % of the ultimate strength of LS1	LS2-FII
CDA-11 %− 1E7	To predict the structural responses with up to 10,000,000 cycles under a load range of 1.1 % to 11 % of the ultimate strength of LS1	LS2-FI
CDA-50 %− 2E6	To predict the structural responses with up to 2,000,000 cycles under a load range of 5 % to 50 % of the ultimate strength of LS1	LS3-F
FEA-Residual	To predict the residual strength of the slab after CDA-50 %− 2E6	LS3-RS

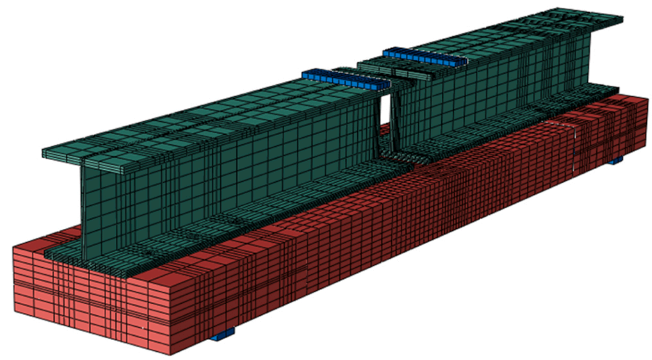

Fig. 8. Creation of FE model of the link slab.

respectively as given in Table 5 according to [21].

The load-deflection curve obtained from the baseline static analysis FEA-S is shown in Fig. 9. The baseline FE model predicted an ultimate strength of 67.5 kN at a midspan deflection of 20.4 mm, which agreed well with test results with an ultimate strength of 67.1 kN at a midspan deflection of 21.1 mm [6]. This shows the accuracy of the baseline FE model so that it is suitable for the subsequent CDA.

4.3. Parameters used in damage models and CDA

The material parameters of the damage model of hybrid ECC used for CDA were summarised in Table 6. In addition, as shown in Fig. 10, values of parameters for the material damage model of steel reinforcement bar, u_β, and v_β, $\beta = I, II, III$ used were obtained by best fitting the residual strains $\varepsilon_{re\text{-}\beta}$ $(\beta = I, II, III)$ from the fatigue test at stress level ranges of $S = 0.5, 0.55$, and 0.6 [25]. The model parameters retrieved were given in Table 7.

For the user defined density factor k used in the CDA (Section 2.1), a sensitivity study was performed with cycle density factors $k = 5, 10,$ and 15. It was found that $k = 10$ should be generally suitable for the analysis of beams and slabs under flexural fatigue loadings [18]. As shown in Fig. 11, the analysis results converged and achieved similar accuracy between $k = 10$ and $k = 15$. However, with the use of a larger value of $k = 15$, the analysis would require a higher number of static equivalent analyses and lead to higher computational costs. Herein, $k = 10$ was used so that a reasonable accuracy could be achieved with a smaller number of equivalent static analyses (J=31, Section 2.1) with less computational cost. For the CDA termination criteria (Section 2.2), based on the similarity between static failure and fatigue failure of the link slab observed in actual tests [6], the midspan deflection at failure $d_T = 20.4$ *mm* observed from the static test LS1-S was employed as the termination criterion for the fatigue failure of the ECC matrix while normalised damage limit $D_{bar,limit} = 1$ was used to capture the fatigue failure of the steel reinforcement bar.

4.4. Estimation of fatigue life of link slabs at different fatigue loading levels

As listed in Table 2, three separate analyses namely, CDA-11 %, CDA-50 %, and CDA-75 % were conducted to estimate the fatigue life of hybrid ECC link slabs under three different fatigue loading levels. The results obtained are summarised in Table 8 and Fig. 12. As shown in Fig. 12a, in the CDA-11 % analysis corresponding to a low fatigue load range from 1.1 % to 11 % of static strength, the damage index of steel reinforcement bar D_{bar} increased as the deformation developed with the increase of applied cycles. It was observed that D_{bar} developed slowly to 0.2 after 2×10^{10} cycles and then increased sharply and reached the damage limit $D_{bar,limit} = 1$ with a predicted fatigue life of $\widetilde{N_{f,M}} = 21{,}978{,}000{,}000$ cycles (i.e., 21 billion cycles). In addition, as shown in Figs. 12b and 12c, analysis CDA-50 % predicted a fatigue life

Table 3
Summary of material properties of hybrid ECCs under compression.

$\sigma_{c0.4}$/MPa	$\varepsilon_{c0.4}$	σ_{c0}/MPa	ε_{c0}	σ_{cl}/MPa	ε_{cl}	σ_{cm}/MPa	ε_{cm}	E/GPa
32.8	1.2×10^{-3}	94.5	0.0048	40	0.006	20	0.034	28.3

Table 4
Summary of material properties of hybrid ECCs under tension.

σ_{t0}/ MPa	ε_{t0}	σ_{t1}/ MPa	ε_{t1}	σ_{tp}/ MPa	ε_{tp}	σ_{tu}/ MPa	ε_{tu}
1.86	6.5×10^{-5}	5.32	0.0024	5.82	0.0206	2.5	0.361

Table 5
Interactions among different parts in link slabs.

	ECC slab	Steel beam	Stud	Steel reinforcement bar
ECC slab	N/A	-	-	-
Steel beam	Hard & Tangential	N/A	-	-
Stud	Hard & Tangential	Tie	N/A	-
Steel reinforcement bar	Embed	N/A	N/A	N/A

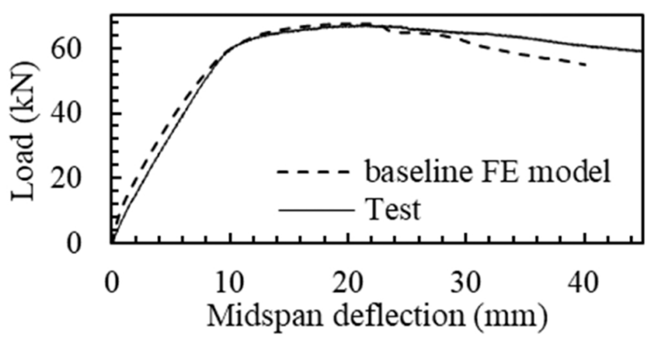

Fig. 9. Load-deformation relations from baseline static FEA-S analysis and LS1-S test.

$\widetilde{N_{f,M}}$= 3,400,000 cycles (i.e., 3.4 million cycles) under a higher fatigue load range of 5 % to 50 % of static strength. For the highest fatigue load range of 7.5 % to 75 % of static strength, analysis CDA-75 % predicted a fatigue life $\widetilde{N_{f,M}}$= 63,360 cycles. It should be noted that all these three analyses were terminated due to the criterion of $D_{bar,J}$> 1 which implied that the failure of the link slabs was due to the fatigue failure of the steel reinforcement bars. Although the fatigue life of the link slab varied from a few thousand cycles to more than 20 billion cycles under different fatigue loading ranges, due to the design of CDA, in all three analyses, only 31 static analyses were used. This demonstrated the efficiency of the CDP procedure.

Since in the experimental study [6], test LS2-FI was terminated at the 10,000,000th cycle and LS3-F was stopped at the 2,000,000th cycle (Table 1), no direct validation for the accuracy of analysis CDA-11 % and analysis CDA-50 % can be carried out. However, it should be noted that both analysis results are actually consistent with the test results. Fatigue life predicted by analysis CDA-11 % (21 billion cycles) is much greater than the 10 million cycles applied in test LS2-FI which showed very little damage and small deflection (1.49 mm, Table 1) at the end of the test [6]. Furthermore, fatigue life predicted by analysis CDA-50 % (3,400,000 cycles) is also consistent and higher than the 2 million cycles applied in test LS3-F which showed moderate damage and deflection (6.43 mm, Table 1).

The accuracy of analysis CDA-75 % was validated by the fatigue test LS2-FII [6]. As shown in Fig. 12c, analysis CDA-75 % well predicted the deformation-cycle relationship compared with test results. It should be noted that the last updated FE model in CDA-11 % analysis was used as the baseline model for CDA-75 % analysis since only very minor damage had been developed in link slab LS2 after 10 million load cycles as shown in Table 1. The CDA-75 % results and test LS2-FII results in terms of fatigue life and failure mode were compared. The predicted fatigue life $\widetilde{N_{f,M}}$ = 63,360 was close to the fatigue life $N_{f,M}$ = 45,317 observed from test LS2-FII. As shown in Fig. 12c, CDA was terminated due to the fatigue failure of the reinforcement bars (i.e., $D_{bar,J}$ >1) rather than the deformation limit as the deflection predicted at reinforcement bar failure was $10.4\ mm < d_T$= 20.4 mm. Such predictions also agreed with the failure mode observed in the fatigue test. In addition, at n = 40,000 as shown in Fig. 13, the distribution of the damage index of the hybrid ECC matrix in terms of the accumulated plastic strain D_ε (Fig. 13a) is similar to the microcracking pattern observed in test LS2-FII (Fig. 13b). It was noted that there relatively fewer medium cracks developed on the left sides in Fig. 13b that differ from the damage prediction in Fig. 13a, which may be caused by material random flaws due to the inhomogeneous property

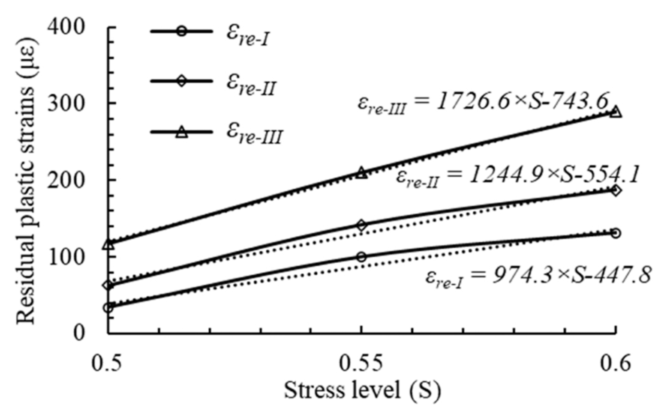

Fig. 10. Residual plastic strains and linear fitting curves.

Table 7
Material parameters of steel reinforcement bar.

$\varepsilon_{re\text{-}\beta}=u_\beta S+v_\beta$ β = I, II, III					
u_I	v_I	u_{II}	v_{II}	u_{III}	v_{III}
974.3	-447.8	1244.9	-554.1	1726.6	-743.6

Table 6
Material parameters of hybrid ECC calibrated by fatigue tests.

$f_m=a_mS^{bm}$		$f_n=a_nS^{bn}$		$f_p=a_pS^{bp}$		$f_q=a_qS^{bq}$		ln (N_f) =c×S+g	
a_m	b_m	a_n	b_n	a_p	b_p	a_q	b_q	c	g
1.05	6.05	2.35	4.46	1.33	6.64	2.75	4.81	-49.02	0.026

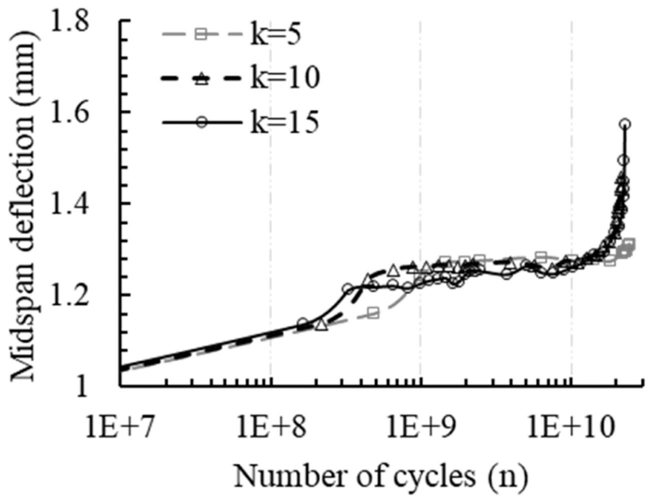

Fig. 11. Sensitivity study of cycle density factor k.

Table 8
Summary of CDA results for CDA-11 %, CAD-50 % and CDA-75 %.

	CDA-11 %	CDA-50 %	CDA-75 %
k, J	$k = 10$, $J = 31$		
$\widetilde{N_{f,M}}$	21,978,000,000	3,400,000	63,360
d_J (mm)	1.48	6.19	10.40
$D_{bar,J}$	> 1	> 1	> 1

of the material and casting quality. A few ECC elements in the midsection developed higher values of damage factor (D_ε>0.5) and highlighted in dark green and red. Since D_ε represented the level of accumulated plastic strains, it reasonably reflected the microcracks observed in the test.

4.5. Prediction of structural responses of link slabs at designated applied cycles

Two analyses with the designated applied cycles prescribed, namely CDA-11 %− 1E7 and CDA-50 %− 2E6 were performed and structural responses such as the deformation-cycle relationship and the development of strains in steel reinforcement bars were investigated. Analysis CDA-11 %− 1E7 was conducted with a designated 10 million load cycles applied. Table 9 summarises analysis results after 10 million load cycles were applied while Fig. 14 compares the deformation-cycle relationship derived from CDA with experiment results. As shown in Fig. 14, the CDA results agreed well with the experimental results. In particular, after 10 million load cycles were applied, CDA predicted a midspan deflection of 1.13 mm while the deflection observed in the test was 1.49 mm. In addition, as shown in Table 9, a small value of reinforcement bar damage index $D_{bar,J}$= 0.00057 was predicted which also agreed with the experimental observation [6].

Analysis CDA-50 %− 2E6 was performed with a designated 2 million load cycles under a higher fatigue load range of 5.0 % to 50 % and corresponding test LS3-F (Table 1). The predicted deformation-cycle relation was again reasonably well agreed with the test results as shown in Fig. 15. A midspan deformation d_J= 5.68 mm was predicted after 2 million load cycles and was slightly less than the deformation observed in the test (6.43 mm). Such a minor discrepancy may be caused by material random flaws and boundary nonlinearity (i.e. gradually damage of materials and then change in the support conditions at the support boundaries due to repeating contact loading) which were not considered in the current simulations. A higher growth rate of predicted deformation was noted at around the 2,000,000th cycle which was also observed in test LS3-F. Regarding the reinforcement bar damage, a moderate value of D_{bar}= 0.43 was predicted.

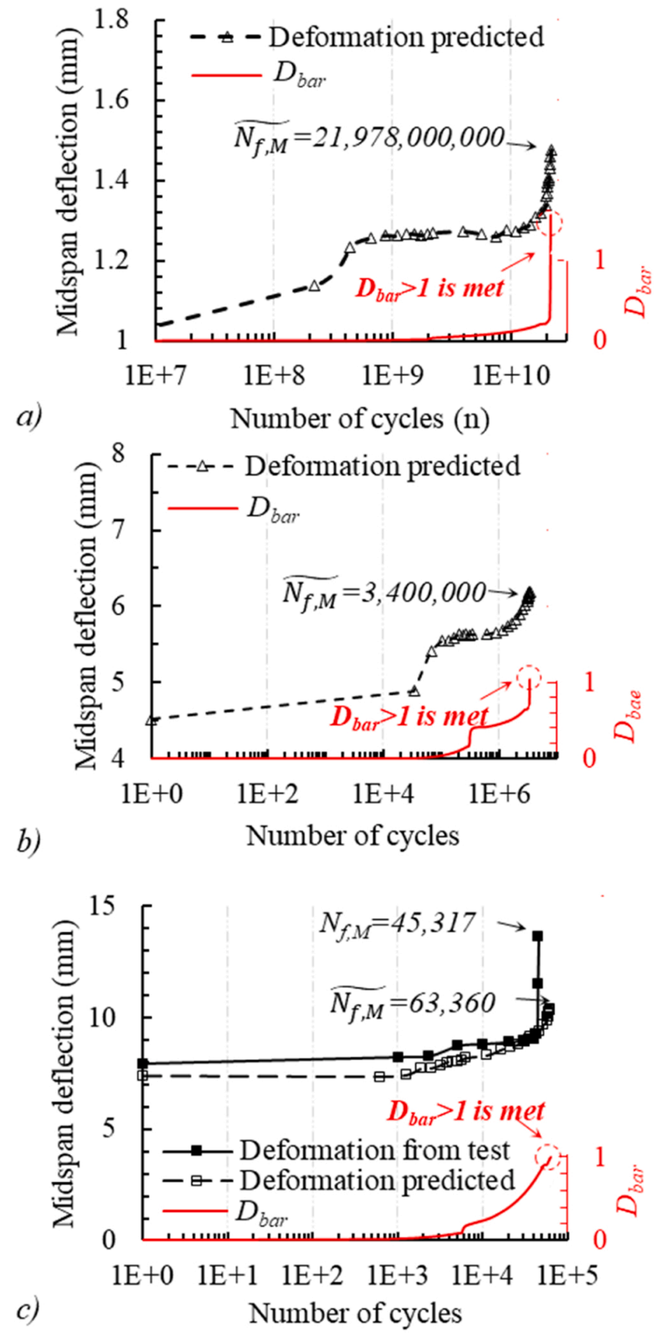

Fig. 12. Fatigue life estimations by a) CDA-11 %, b) CDA-50 %, and c) CDA-75 %.

Fig. 16 shows the development of strains of steel reinforcement bars from both analysis CDA-50 %− 2E6 and test measurement. As shown in Fig. 16a, the strains observed from the test were monitored by six strain gauges (S1-S6) installed on steel reinforcement bars in slab LS3 [6]. Strain predictions from analysis CDA-50 %− 2E6 analysis were retrieved at the same positions where strain gauges S1-S6 were installed (Fig. 16a). As shown in Fig. 16b, strains predicted at S5 and S6 well agreed with the strains observed in tests. For other strain gauge locations, though it was found the predicted strains were generally 10 to 20 % less than the test results, they still followed a similar development trend. For example, the strain at gauge S3 was increased from 1421 με (1st cycle) to 2441 με (2,000,000th cycle) in analysis CDA-50 %− 2E6, while the strain at S3 observed in test LS3-F was increased from 1744 με

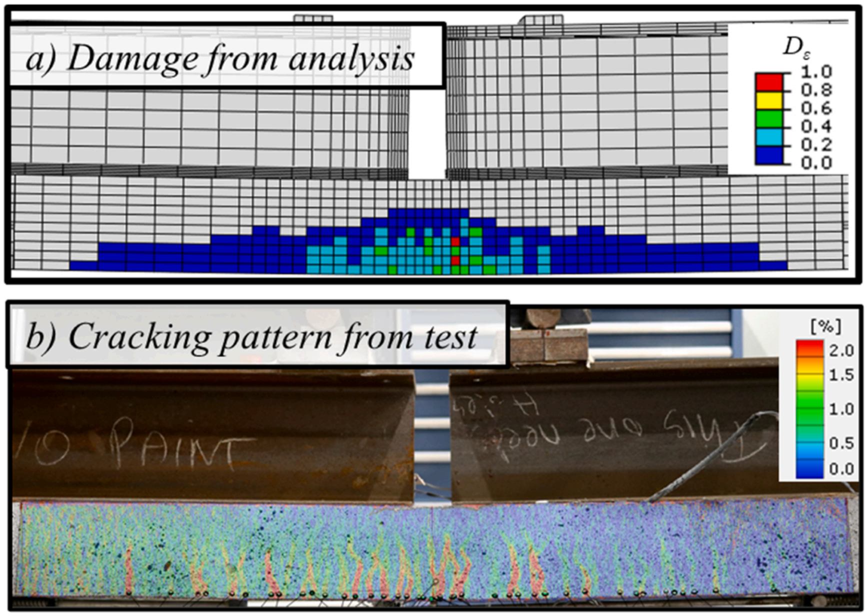

Fig. 13. Comparison of distribution of damage index D_ε from analysis CDA-75 % with the cracking pattern from LS2-FII test at loading cycle n=40,000.

Table 9
Summary of analysis results of CDA-11 %– 1E7 and CDA-50 %– 2E6.

	CDA-11 %– 1E7	CDA-50 %– 2E6
N_J	10,000,000	2,000,000
d_J (mm)	1.13	5.68
$D_{bar,J}$	0.00057	0.43

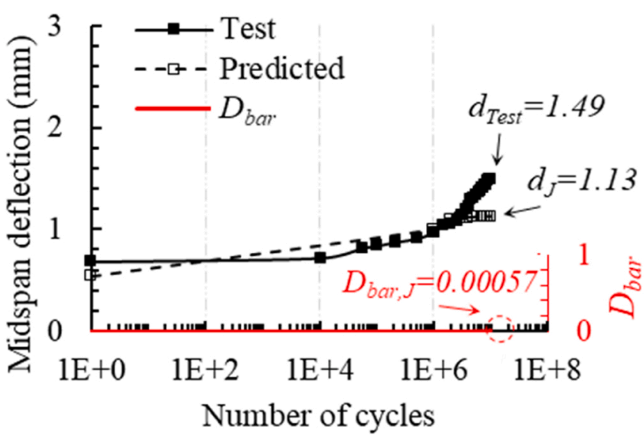

Fig. 14. Deformation-cycle relations from CDA-11 %– 1E7 prediction and LS2-FI test.

(1st cycle) to 2770 με (2,000,000th cycle). Given that FE analysis generally is less accurate for stress/strain prediction and the CDA replaced the detailed fatigue analysis with a very small number of equivalent static analyses, such differences between CDA strain and test results are reasonable and acceptable.

4.6. Residual strength prediction

A static FE analysis (FEA-Residual) was performed following the analysis CDA-50 %– 2E6 to predict the residual strength of the link slab after sustained 2 million load cycles with a load range of 5 % to 50 % of the static strength. In the analysis FEA-Residual, in order to simulate the actual residual strength test [6], the last updated FE model from analysis

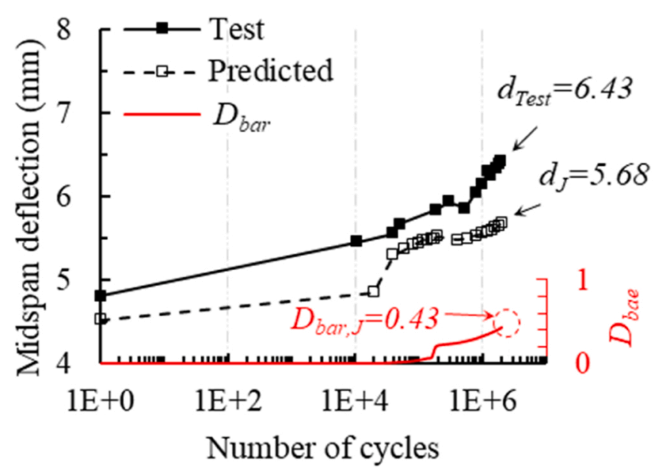

Fig. 15. Deformation-cycle relations from CDA-50 %– 2E6 prediction and LS3-F test.

CDA-50 %– 2E6 was exported for static analysis. Loading was then reset to zero and increased by displacement control until the link slab failed. Fig. 17 compared the load-deformation relation obtained from the analysis FEA-Residual with the residual strength test results. It was noted that the starting point of the experimental load-deformation curve was offset along the displacement axis for a value of d_o= 3.71 mm, which was the residual plastic deformation observed after the fatigue test. Similarly, for the analysis curve, it was also offset for a distance $d_{o,FE}$= 4.43 mm which was the residual plastic deformation predicted by analysis CDA-50 %– 2E6 after 2 million cycles of loading. As shown in Fig. 17, the predicted residual strength was 67.4 kN while the residual strength observed from the test was 67.7 kN. In general, the predicted load-deformation curve and the residual strength agreed well with the test results. This demonstrated that besides predicting the fatigue behaviours and damage of the link slab, the proposed CDA procedure could also lead to a reasonable prediction of the slab's residual strength.

5. Conclusions

In this study, a novel and efficient cycle-driven analysis (CDA)

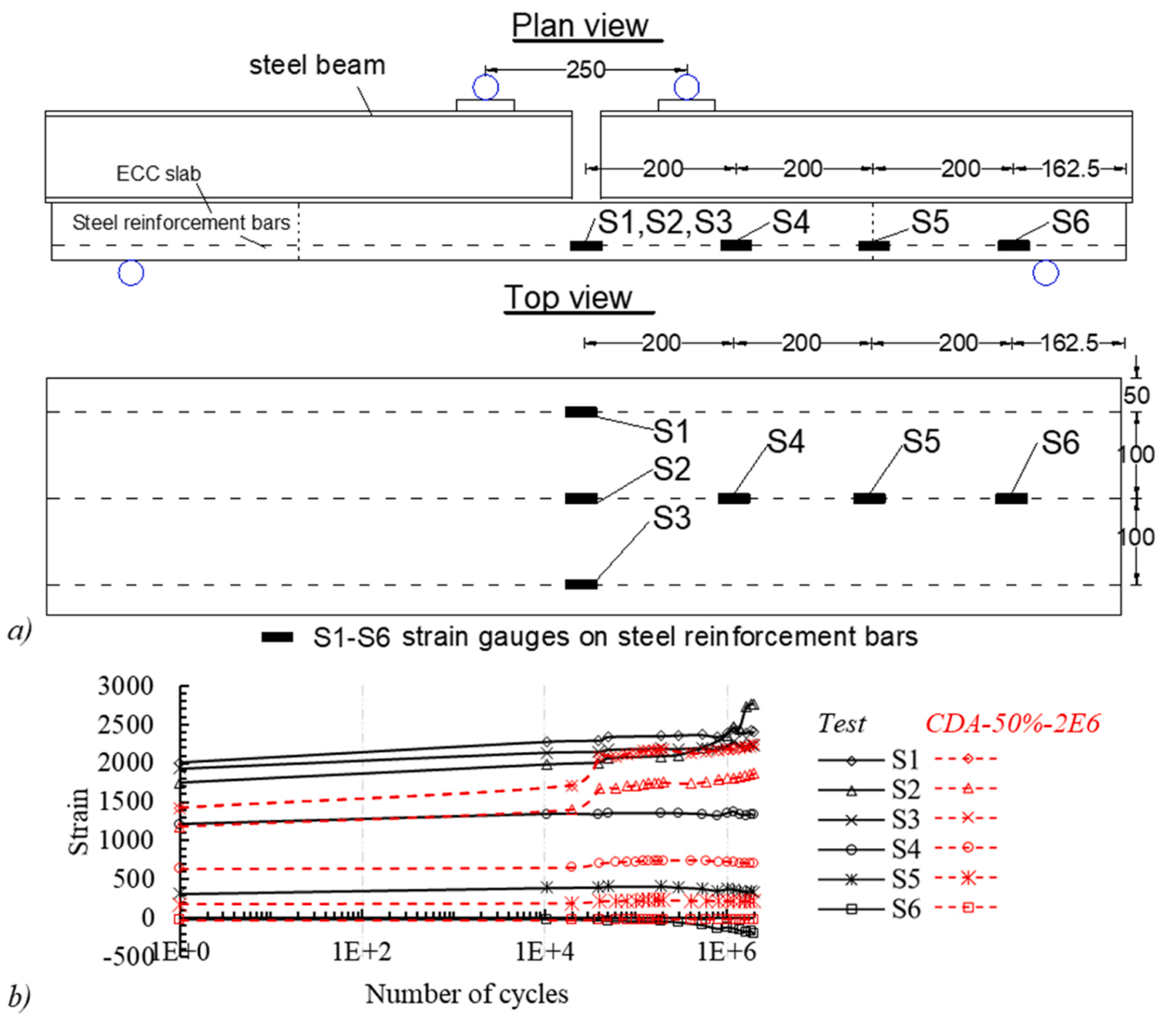

Fig. 16. a) Strain gauges placement and b) strains development in steel reinforcement bars obtained from CDA-50 %– 2E6 and LS3-F test.

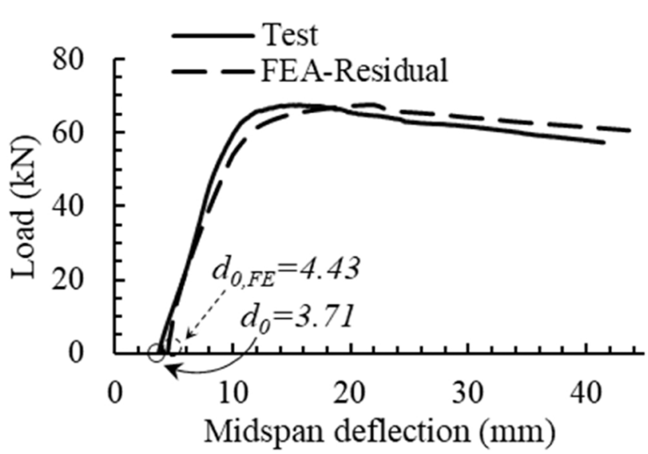

Fig. 17. Load-deformation relations from FEA-Residual analysis and test.

procedure was developed and used for the first time to conduct a detailed structural analysis on the fatigue performance of hybrid Engineered Cementitious Composite (hybrid ECC) link slabs by using a very reasonable amount of computational resources. This proposed CDA procedure replaced expensive cycle-by-cycle analysis with a small number (<50) of equivalent static finite element (FE) analyses. It allows engineers to quickly estimate the fatigue life, the deflection-cycle history as well as the damage pattern development history of the link slab. Furthermore, it also allows engineers to estimate the residual static strength of the slab after a designated number of fatigue loading cycles are applied.

In order to implement the proposed CDA procedure for practical link slab configuration, the damage model developed previously by Zhu et al. [18] was employed and a damage model for the steel reinforcement bar was proposed. Furthermore, to validate the accuracy and reliability of the proposed CDA procedure, a series of CDA models which were corresponding to the flexural fatigue tests conducted in Zhu's experimental study [6], were created. Three models corresponding to different fatigue loading ranges (1.1–11 %, 5–50 % and 7.5–75 % of the static strength of the hybrid ECC link slab) were created and their fatigue life were predicted. Comparison of the modelling results with the experimental results indicated that the proposed model provided consistent fatigue life predictions. More detailed investigations of the modelling results also showed that the proposed procedure successfully predicted the failure modes of the slabs and the damage patterns development histories of both the ECC matrix and the steel reinforcement bars. Furthermore, the proposed CDA procedure was also employed to estimate the residual flexural strength of a moderately damaged link slab after it was subjected to two million fatigue load cycles corresponding to 5–50 % of the slab's static strength. It was found that when comparing with the load-deflection curve obtained from the residual strength test of the damaged slab, the proposed CDA procedure predicted a very similar residual load-deflection curve with an accurate prediction of the residual static strength.

One potential extension of the current work is to conduct a parametric study to investigate the effect of material properties, reinforcement bar ratios and slab geometry on the fatigue performance of the link slabs. Further consideration of material random flaws and boundary nonlinearity in the numerical model may improve the reliability and accuracy of the analysis. Since the proposed CDA procedure is highly efficient and only requires very reasonable computational resource, it could be employed to optimise the link slab design by allowing engineer to assess the performance of a large number of alternative designs within a practical time frame.

CRediT authorship contribution statement

Shiyao Zhu: Formal analysis, Investigation, Methodology, Software, Validation, Visualization, Writing – original draft. **Yixia Zhang:** Methodology, Supervision, Writing – review & editing. **Chi King Lee:** Conceptualization, Investigation, Methodology, Resources, Supervision, Writing – review & editing.

Declaration of Competing Interest

The authors declare that they have no known competing financial interests or personal relationships that could have appeared to influence the work reported in this paper.

Acknowledgements

UNSW Canberra's support for the first author to conduce this research received through TFS Scholarship are gratefully acknowledged.

References

[1] Li VC. Introduction to engineered cementitious composites (ECC). Engineered cementitious composites (ECC). Berlin, Heidelberg: Springer; 2019.
[2] Chu K, Hossain KMA, Lachemi M. Static and fatigue behaviour of ECC link slabs in reinforced concrete girder joint-free bridges. Structures 2022;41:1301–10.
[3] Hou MJ, Hu KX, Yu JT, Dong SW, Xu SL. Experimental study on ultra-high ductility cementitious composites applied to link slabs for jointless bridge decks. Compos Struct 2018;204:167–77.
[4] Zhu S, Zhang YX, Lee CK. Polyethylene-steel fibre engineered cementitious composites for bridge link slab application. Structures 2021;32:1763–76.
[5] Zhu S, Zhang YX, Lee CK. Experimental Investigation of Flexural Behaviours of Hybrid Engineered Cementitious Composite Beams under Static and Fatigue Loading. Eng Struct 2022;262:114369.
[6] Zhu S, Zhang YX, Lee CK. An experimental study on hybrid fibre reinforced engineered cementitious composite link slabs under static and fatigue loadings. Eng Struct 2024;300:117254. https://doi.org/10.1016/j.engstruct.2023.117254.
[7] Qian SZ, Li VC, Zhang H, Keoleian GA. Life cycle analysis of pavement overlays made with engineered cementitious composites. cement and concrete. Composites 2013;35:78–88.
[8] Chu K, Hossain KMA, Lachemi M. Experimental and numerical study on joint-free bridges with steel or GFRP-reinforced ECC link slab subjected to static loading. Constr Build Mater 2022;327:127035.
[9] Zhu L, Wang JJ, Li X, Tang L, Yu BY. Experimental and numerical study of curved SFRC and ECC composite beams with various connectors. Thin Walled Struct 2020;155:106938.
[10] Mahmud GH, Yang Z, Hassan AMT. Experimental and numerical studies of size effects of ultra high performance steel fibre reinforced concrete (UHPFRC) beams. Constr Build Mater 2013;48:1027–34.
[11] Jendele L, Cervenka J. Finite element modelling of reinforcement with bond. Comput Struct 2006;84:1780–91.
[12] Bradford MA, Manh HV, Gilbert RI. Numerical analysis of continuous composite beams under service loading. Adv Struct Eng 2002;5:1–12.
[13] Kwak HG, Filippou FC. Finite element analysis of reinforced concrete structures under monotonic loads: department of civil engineering. University of California; 1990.
[14] Tong L, Liu B, Zhao XL. Numerical study of fatigue behaviour of steel reinforced concrete (SRC) beams. Eng Fract Mech 2017;178:477–96.
[15] Liu F, Yu C, Yi W. Study on equivalent static method for the analysis of fatigue behavior of reinforced concrete beam. E3S Web Conf 2021;272:02018.
[16] Cachim P. Numerical modelling of fibre-reinforced concrete fatigue in bending. Int J Fatigue 2002;24:381–7.
[17] Banjara Nawal K, Ramanjaneyulu K. Experimental investigations and numerical simulations on the flexural fatigue behavior of plain and fiber-reinforced concrete. J Mater Civ Eng 2018;30:04018151.
[18] Zhu S, Zhang YX, Lee CK. A new finite element procedure for simulation of flexural fatigue behaviours of hybrid engineered cementitious composite beams. Eng Struct 2022;269:114839.
[19] Suthiwarapirak P, Matsumoto T, Kanda T. Multiple cracking and fiber bridging characteristics of engineered cementitious composites under fatigue flexure. J Mater Civ Eng 2004;16:433–43.
[20] Dassault Systemes. Abaqus user subroutines reference guide, dassault systemes. Providence, RI, USA; 2014.
[21] Zhu S, Zhang YX, Lee CK. Finite element analysis of hybrid fiber reinforced engineered cementitious composite link slabs. Int J Comput Methods 2022:2143022.
[22] ASTM C39 / C39M-18. Standard test method for compressive strength of cylindrical concrete specimens. ASTM International, West Conshohocken, PA 2018 (www.Astm.Org).
[23] ASTM C1273-18. Standard test method for tensile strength of monolithic advanced ceramics at ambient temperatures. ASTM International, West Conshohocken, PA 2018 (www.Astm.Org).
[24] Wang C, Shen Y, Zou Y, Zhuang Y, Li T. Analysis of mechanical characteristics of steel-concrete composite flat link slab on simply-supported beam bridge. KSCE J Civ Eng 2019;23:3571–80.
[25] Zhang D, Huang W, Zhang J, Jin W, Dong Y. Prediction of fatigue damage in ribbed steel bars under cyclic loading with a magneto-mechanical coupling model. J Magn Magn Mater 2021;530:167943.
[26] Standards Association of Australia, Committee B. D. Concrete structures. Concrete structures: AS 3600-2018. Homebush, N.S.W.: Standards Australia; 2018.